# NUMERICAL INVESTIGATION OF TURBULENT CONVECTION HEAT TRANSFER IN POROUS MEDIA COMPOSED OF ROUGH SOLID OBSTACLES

Vishal Srikanth<sup>1</sup>, Andrey V. Kuznetsov<sup>1\*</sup>

<sup>1</sup>Department of Mechanical and Aerospace Engineering, North Carolina State University Raleigh, NC 27695-7910, USA

## **ABSTRACT**

Porous media heat exchangers can facilitate efficient transfer and reliable storage of heat, which is essential to keep up with the growing demand for renewable energy. Turbulence transport in porous media is determined by the geometry of the solid obstacles at the microscale. The focus of the present study is to understand the influence of solid obstacle surface roughness on the heat transfer characteristics of the porous medium through a systematic study. Surface roughness is often unavoidable during fabrication, or it can develop over time due to corrosion, and it is an important consideration in design. In this study, the Reynolds-averaged microscale flow field is simulated by explicitly representing the surface roughness geometry by adding square roughness particles on the solid obstacle. The roughness particle height and spacing, the porosity, and the Reynolds number are varied systematically. The trends of the macroscale variables such as the pressure drag, viscous drag, and surface averaged Nusselt number with respect to the roughness particle height and spacing are analyzed. The primary focus of the analysis is the microscale flow physics caused by the roughness particles that is underlying in the macroscale variables.

We have identified two distinct flow regimes for the variation of surface roughness particle height ( $k_s$ ) and spacing (w). The roughness particles cause the formation of recirculation vortices that are similar in size to the roughness particle height. Roughness particle heights of  $k_s = 0.01d$  and 0.005d (where d is the solid obstacle hydraulic diameter) are considered fine roughness whose influence on heat transfer is limited to the change in the width of the boundary layer, causing a heat transfer decrease compared to the smooth case. Roughness particle heights of  $k_s = 0.1d$  and 0.05d are considered coarse roughness because they modify the geometry of the solid obstacle and the flow patterns around them, causing a heat transfer enhancement. Increase in the roughness particle spacing increases the tortuosity of the flow, but the number of roughness particles on the surface decreases. The two competing factors gives rise to two regimes, which transition from the prevalence of roughness to smoothness. We also note that the effect of surface roughness is enhanced when the porosity is lowered and the Reynolds number is increased. The study concludes that the surface roughness of solid obstacles in porous media should be small and sparsely distributed to decrease its detrimental effects on heat transfer.

KEY WORDS: forced convection, RANS, numerical simulation

#### 1. INTRODUCTION

Surface roughness is frequently encountered in practical applications of both natural and engineered porous media. Roughness can be unavoidable during manufacturing, or it can develop over time due to damage, corrosion, and scale formation. The results shown in the paper show how the surface roughness of the microscale solid obstacle that form the porous medium modifies the drag force and the Nusselt number on the solid obstacle surface. The influence of the solid obstacle surface roughness is especially relevant in porous media since its effect is compounded over the numerous solid obstacles that are present in the porous medium. There are very few studies that consider solid obstacle surface roughness in porous media. Several researchers have investigated laminar single and multi- phase flow with a focus on how surface roughness influences flow in soil and porous rocks. In these studies[1–3], the solid obstacle surface roughness has been shown to cause flow retardation in the pore space. For single phase laminar flow in porous media, surface roughness influences the permeability according to the

<sup>\*</sup>Corresponding Author: avkuznet@ncsu.edu

pore size and the roughness height [4]. Studies of fractal [5] and sinusoidal [6] surface roughness in porous media show that surface roughness decreases permeability, where roughness introduces increased inertial effects and viscous dissipation. Surface roughness has been shown to improve heat transfer in tube banks, which are an example of a porous medium, by using small roughness particles on the solid obstacle surface [7]. We have defined the term roughness particles as the solid particles located on the surface of the solid obstacles that make the surface rough. To the authors' best knowledge, there are no comprehensive studies on the effect of solid obstacle surface roughness on turbulent heat transfer in porous media.

There are numerous studies of surface roughness for flows in channels and around bluff bodies. In channel flows, roughness has been shown to both increase [8–10] and decrease drag [11] depending on the roughness particle geometry. Heat transfer enhancement is often experienced when using surface roughness particles on the channel walls [12,13]. For flow around cylinders, some studies report that roughness causes early transition to turbulence and flow separation [14–16], whereas others report compact wakes as a result of surface roughness [17]. Surface roughness on cylinder walls has been shown to decrease heat transfer [18], although it should be noted that the roughness particles in ref. [18] created deep trenches in the cylinder's surface.

Contrasting observations of drag increase and reduction, as well as heat transfer enhancement and reduction, are frequently reported in the literature. There is a strong dependence of the flow properties on the geometry of the roughness particles: the roughness particle size, spacing, and shape. In this paper, we undertake a comprehensively study of the microscale and macroscale flow features introduced by roughness particles. We systematically vary the roughness particle height, spacing, porosity, and the Reynolds number. The details of the geometry used to simulate the porous medium are described in section 2.1. The numerical procedure is described in section 2.2, followed by a validation study in section 2.3. The results are discussed in section 3.

# 2. SOLUTION METHOD

In the present study, the Reynolds averaged flow field inside the porous medium is calculated by using the commercial code Ansys® Academic Research Fluent, Release 17.0. The solid obstacles in the porous medium are explicitly modeled. Constant temperature is assumed throughout the solid obstacle volume and at the surface of the solid obstacle.

2.1 Computational Geometry In this paper, an infinitely spanning porous medium is represented by using an in-line arrangement of square cylinder solid obstacles. The computational geometry is twodimensional since the Reynolds Averaged Navier Stokes (RANS) approach is used. For cylindrical solid obstacles, the Reynolds averaged flow field components in the axial direction will be zero. Only one solid obstacle is used in the Representative Elementary Volume (REV) since the solution to the RANS equations will be identical around all of the solid obstacles in the periodic domain due to a lack of variation in the solid obstacle geometry. Square roughness particles are placed on the surface of the square cylinder to simulate solid obstacle surface roughness. The resulting computational geometry is shown in Fig. 1. In practical scenarios, the geometry of the porous medium and the roughness elements are often randomly shaped and distributed. However, regular solid obstacle geometries are used in the present work for the following reasons: (1) the high computational cost of simulating an ensemble of randomized solid obstacle geometries and (2) the complexity associated with statistically analyzing the microscale flow for the ensemble of solid obstacle geometries. Regular solid obstacle geometries are commonly used in numerical studies of both porous media flows [19,20] and roughness flows [9,18]. Regular solid obstacle geometries enable us to qualitatively study the important flow features that emerge from the inclusion of roughness elements and understand how they influence heat transfer.

We have set the hydraulic diameter of the smooth solid obstacle (d) to be equal to 1 to non-dimensionalize the length scales. Therefore, all distances are reported as a ratio to the hydraulic

diameter. The roughness particle height  $(k_s)$  is equal to the side length of the square roughness particle. The roughness particle spacing (w) is equal to the distance between the centers of two adjacent roughness particles. The number of roughness particles  $(n_p)$  along one side length of the solid obstacle is equal to d/w. The pore size (s) varies for each case so that the porosity  $(\phi)$  of the porous medium is set to a fixed value (equation 1):

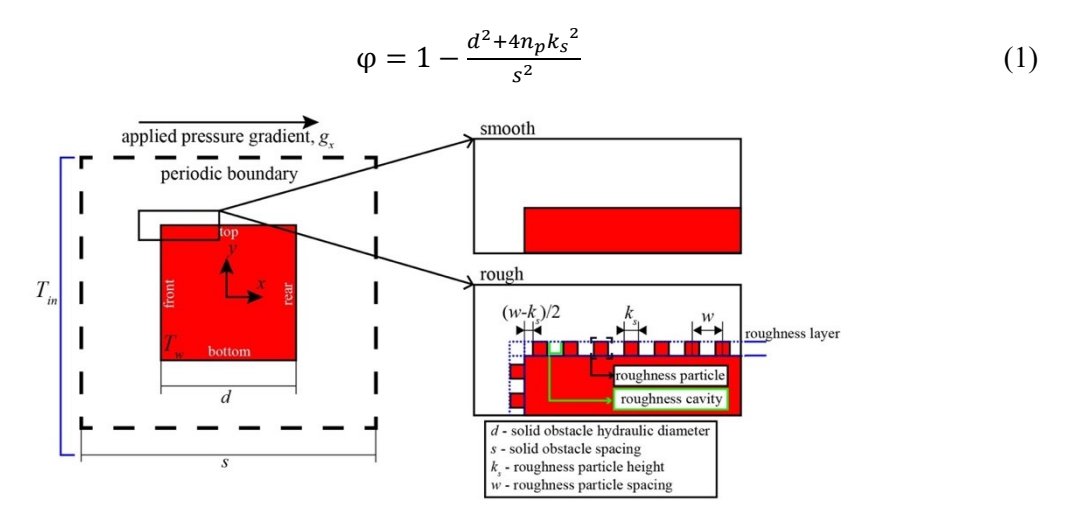


Fig. 1 The computational geometry used to calculate the Reynolds averaged flow solution in periodic porous media with rough and smooth solid obstacles.

**2.2 Details of the Numerical Method** The flow through the periodic porous medium is sustained by applying an external pressure gradient term in the flow direction  $(g_x)$ . The temperature at the solid obstacle surface  $(T_w)$  is set equal to 350 K. The bulk temperature of the fluid that enters the periodic domain  $(T_{in})$  is 300 K. Note that the fluid is heated by the solid obstacle and the microscale temperature distribution is not periodic in the flow direction. The thermal conductivity of the fluid  $(\lambda)$  is 0.0242 W/m-K and the specific heat of the fluid  $(C_P)$  is 1006.43 J/Kg-K. The microscale temperature distribution is periodic in the y direction. The microscale velocity and pressure distributions are periodic in x and y directions. The RANS equations are solved along with the realizable k- $\epsilon$  model [21] to predict the turbulence viscosity. The two-layer k- $\epsilon$ , k-l near wall treatment [22] is used to improve accuracy at the wall by avoiding the direct specification of turbulence dissipation rate. The governing equations and the model constants are available in the ANSYS theory guide [23].

The governing equations are solved by using the finite volume method. The spatial derivatives are discretized using the second-order accurate upwind difference scheme for the convective terms and the second-order accurate central difference scheme for the diffusive terms. The pressure is stored at the centroid of the face of the computational grid cells, staggered from the location of the velocity and temperature variables stored at the centroid of the cell volume. The governing equations are solved in a segregated manner using the SIMPLE algorithm. The density of the fluid  $(\rho)$  is set equal to 1 and the dynamic viscosity  $(\mu)$  is set equal to 1/Re, where Re is the Reynolds number. The Reynolds number is defined in equation 2:

$$Re = \frac{\rho u_m d}{\mu} \tag{2}$$

where  $u_m$  is the Reynolds averaged, superficially (over the whole volume) averaged x- velocity. The value of  $g_x$  is iteratively adjusted such that  $u_m$  is equal to 1. Therefore, the governing equations for the conservation of momentum are non-dimensional. The flow in the porous medium is assumed to be turbulent since turbulence is commonly encountered in convection-assisted heat exchangers and thermal energy storage devices [24,25].

The numerical method has been validated against the direct numerical simulation (DNS) results of Chu et al. [26] for the turbulent flow through a periodic porous medium. In the validation case, the porous medium consists of square cylinder obstacles arranged in a staggered manner. The porosity is 0.75 and the Reynolds number is 1000. We observed excellent qualitative agreement between the flow fields predicted by the realizable k- $\epsilon$  RANS model (Fig. 2(a)) and by DNS results. Both the RANS and DNS flow fields consisted of the following features: a single flow stagnation at the front of the solid obstacle, two flow separation points at the rear of the solid obstacles, microscale vortices following flow separation, and shear flow between horizontal surfaces of two neighboring solid obstacles. Quantitatively, the RANS model underpredicts the size of the microscale vortices as indicated by higher velocity in the wake compared to DNS (Fig. 2(b)). Based on the grid dependence of the velocity distribution, we have used a grid size ( $\Delta x/d$ ) of 0.03 in subsequent simulations (Fig. 2(b)).

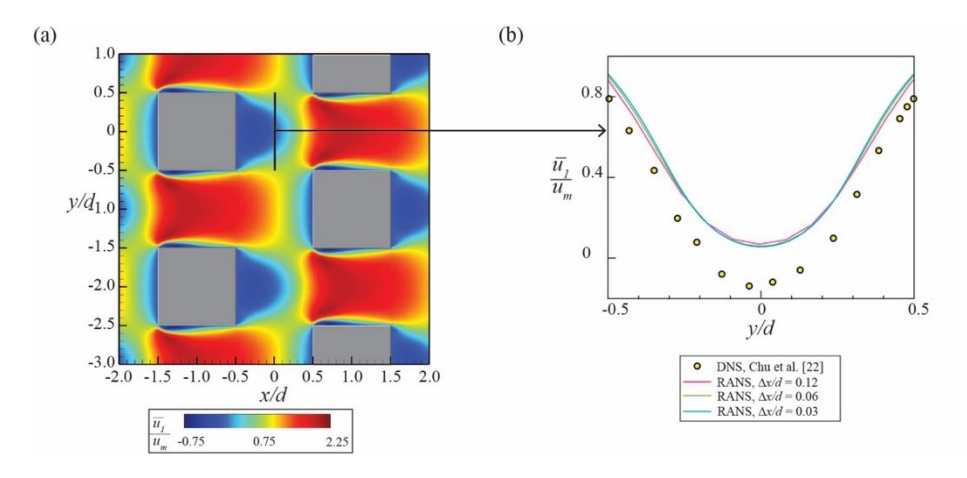


Fig. 2 (a) x- velocity distribution predicted by the realizable k- $\varepsilon$  RANS model. (b) velocity profile comparison between RANS and DNS for different grid sizes plotted at the black line shown in (a).

## 3. RESULTS AND DISCUSSION

The influence of the two roughness parameters: roughness particle height and spacing, on the flow inside porous media are studied independently. The shape and the aspect ratio of the roughness particle are kept the same across all the cases. In porous medium flows, the porosity and the Reynolds number are important parameters since they modify the boundary layer formed between the solid obstacles as well as the flow features in the pore volume. The discussion has been divided into the following two sections that focus on the influence of the variation of  $k_s$  and w on turbulent heat transfer in porous media.

3.1 Surface Roughness Particle Height ( $k_s$ ) The surface roughness particle height determines the extent to which the roughness particles protrude into the boundary layer in between the solid obstacles. First, the roughness particle height has been set to the following values: 0.005, 0.01, 0.05, and 0.1. The roughness particle spacing was set equal to  $w = 2k_s$ . The Reynolds number of the flow is set equal to 1000. The porosity of the porous medium is set to the following values: 0.5, 0.65, and 0.8. The three values of porosity represent three different flow regimes observed in porous media. The flow regimes are formed when the porosity increases because the pore volume increases, which increases the volume over which the microscale vortices develop. At low porosity ( $\varphi = 0.5$ ), recirculating vortices are formed in the pore volume, whereas at high porosity ( $\varphi = 0.8$ ), shedding vortices are formed [27].

The pressure ( $F_{pressure}$ ) and viscous ( $F_{viscous}$ ) drag forces and the surface averaged Nusselt number (Nu) are the primary variables that dictate flow and heat transfer properties in the present case of periodic porous media. The surface averaged Nusselt number (Nu) is calculated by using the surface averaged heat flux ( $q''_w$ ) as shown in equation 3:

$$Nu = \frac{4q''_w(d+2n_pk_s)}{(T_w - T_{in})\lambda} \tag{3}$$

The perimeter of the solid obstacle is chosen as the characteristic length scale in equation 3 to avoid a jump discontinuity in Nu between the smooth and rough solid obstacles. The pressure drag force increases when the roughness particle height increases for all the values of porosity we tested (Fig. 3(a)). The increase of  $F_{pressure}$  with  $k_s$  is exponentially higher at lower values of porosity. With the exception of the case of  $k_s = 0.005$  and  $\varphi = 0.8$ , the pressure drag force for the rough solid obstacle is higher than that for the smooth solid obstacle. The viscous drag force decreases when the roughness particle height increases for  $\varphi = 0.8$  and 0.65, but it increases for  $\varphi = 0.5$  (Fig. 3(b)). However, the viscous drag is always less for the rough solid obstacles than that for the smooth solid obstacles. The surface averaged Nusselt number increases when the roughness particle height increases (Fig. 3(c)). It should be noted that the roughness particles increase the surface area of the solid obstacle by a factor of 2 when  $w = 2k_s$ . Heat transfer enhancement by rough solid obstacles is accompanied by a commensurate increase in the drag force. The superficially averaged turbulence kinetic energy increases when the roughness particle height increases (Fig. 3(d)).

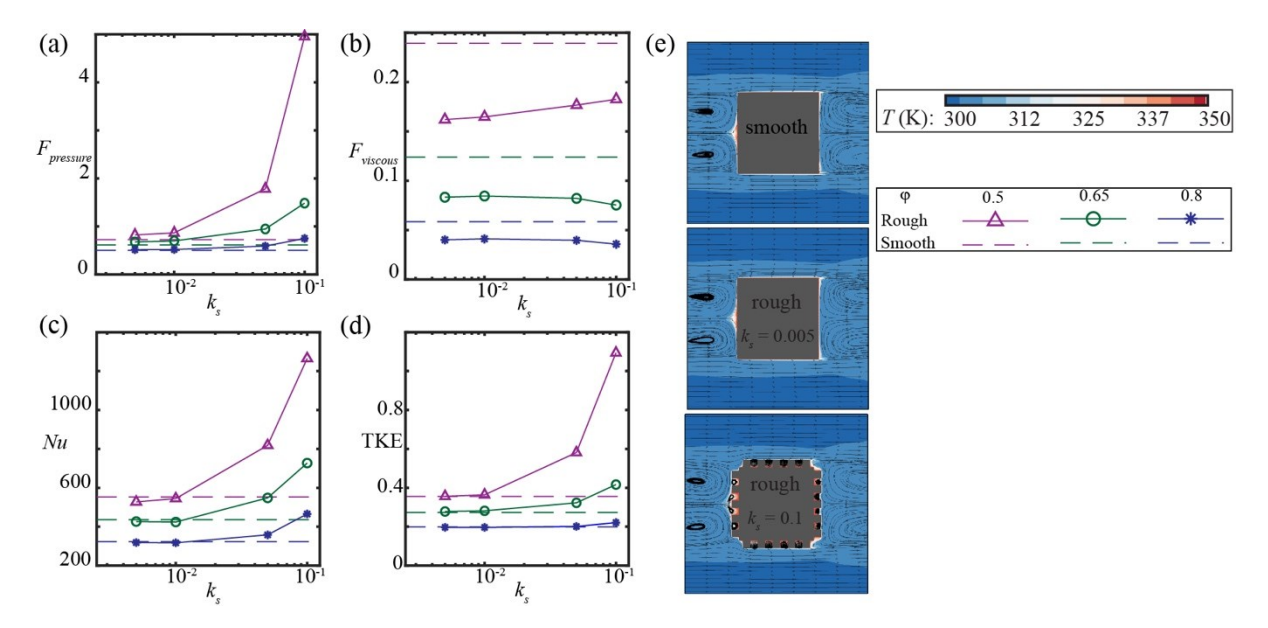


**Fig. 3** The variation of (a) the pressure drag force ( $F_{pressure}$ ), (b) the viscous drag force ( $F_{viscous}$ ), (c) the surface averaged Nusselt number (Nu), and (d) the superficially averaged turbulence kinetic energy (TKE) with the surface roughness particle height ( $k_s$ ). (e) The microscale temperature distribution surrounding smooth and rough solid obstacles.

When the solid obstacle surface is rough, recirculating vortices are formed in between the roughness particles (Fig. 3(e)). In addition, the roughness particles protrude into the pore volume and decrease the cross-section area through which the flow occurs. Therefore, the pressure drag increases as a result of the protrusion due to the increase in the flow stagnation pressure formed at the front face of the roughness particle. Viscous drag decreases due to the decrease in the wall normal velocity gradient caused by flow recirculation in the roughness layer. Flow recirculation also acts as a thermal insulator on the surface of the rough solid obstacles and decreases the surface averaged heat flux. For  $k_s = 0.005$  and 0.01, the high temperature fluid in the roughness layer decreases the wall normal temperature gradient, and consequently the Nusselt number. For  $k_s = 0.05$  and 0.1, the recirculating vortices caused by the roughness particles are large enough to entrain low temperature fluid from above the roughness layer and induce mixing. As a result, heat transfer enhancement is observed in these cases when compared to the smooth case. On this basis, we define two regimes of surface roughness with respect to the roughness particle height. In the fine roughness regime ( $k_s = 0.005$  and 0.01), the roughness particles are small and numerous, and primarily influence the microscale flow in the roughness layer.

In the coarse roughness regime ( $k_s = 0.05$  and 0.1), the roughness particles are large enough to modify the shape of the solid obstacle. The influence of the roughness particles extends beyond the roughness layer to the entire pore volume. The superficially averaged turbulence kinetic energy increases substantially only at high roughness particle heights and low porosity. Therefore, the turbulence kinetic energy is primarily dependent on the distance between the solid obstacle surfaces, rather than the flow over the surface roughness particles.

Next, the Reynolds number of the flow is set to the following values: 1000, 5000, and 10000. The roughness particle height is set to 0.005 and 0.1 to represent the fine and coarse roughness regimes, respectively. The roughness particle spacing was set equal to  $w = 2k_s$  and the porosity is 0.8. The Reynolds number of the flow is changed by changing the dynamic viscosity of the fluid as described in section 2.2. Both the pressure and viscous drag forces decrease when the Reynolds number is increased (Fig. 4(a) and (b)). The Nusselt number increases when the Reynolds number is increased due to the decrease in the thermal boundary layer thickness (Fig. 4(c)). Increasing the Reynolds number increases the heat transfer reduction in the fine roughness regime. The decrease in the thermal boundary layer width with the increase in Reynolds number is limited by the height of the roughness layer in the fine roughness regime. Increasing the Reynolds number increases the heat transfer enhancement in the coarse roughness regime. The thermal boundary layer width inside the roughness cavity decreases resulting in higher heat flux from the solid obstacle surface area inside the roughness cavity to the flow above it. The distinction in the heat transfer behavior between fine and coarse roughness regimes is caused by the relation between the roughness particle height and the thermal boundary layer width. The superficially averaged turbulence kinetic energy decreases when the Reynolds number increases in both the smooth and rough cases, but it is not shown since there is no qualitative change in the trends.

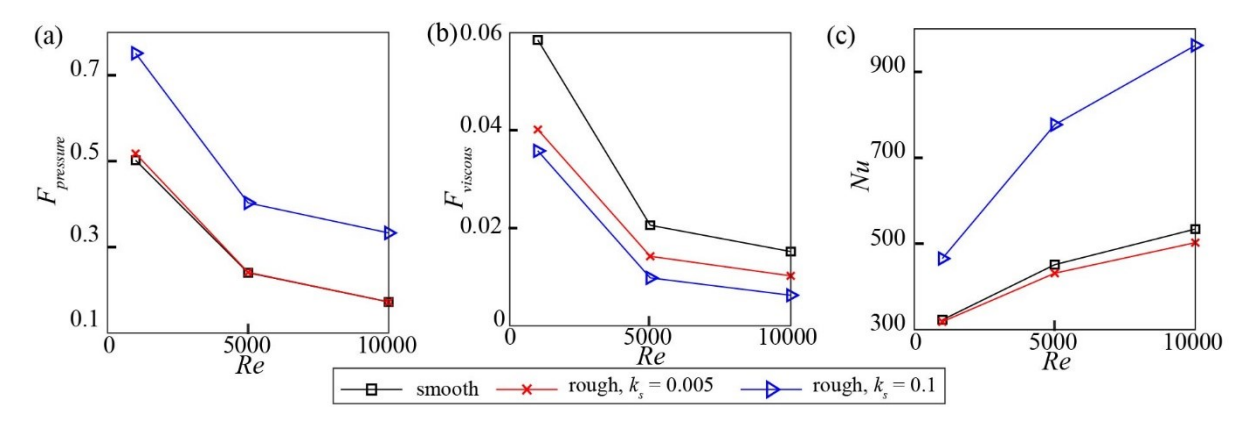


**Fig. 4** The (a) pressure and (b) viscous drag forces decrease when Reynolds number increases, whereas (c) Nusselt number increases when Reynolds number increases.

**3.2 Surface Roughness Particle Spacing** The roughness particle spacing (w) determines the number of roughness particles that are present on the solid obstacle surface and the flow properties inside the roughness cavity. In this study, the roughness particle height is set to  $k_s = 0.01$  to avoid the problem of too few roughness particles on the solid obstacle surface. The roughness particle spacing is set to the following values:  $2k_s$ ,  $4k_s$ ,  $8.33k_s$ , and  $16.67k_s$ . These numbers are chosen to avoid fractional roughness particles on the solid obstacle surface. The Reynolds number is set to 1000 and the porosity is set to the following values: 0.5, 0.65, and 0.8. The variation of the flow properties is non-monotonic when the roughness particle spacing is increased. The pressure drag force first increases and is followed by a decrease when w is increased (Fig. 5(a)). The viscous drag force and the Nusselt number both decrease and are then followed by increase when w is increased (Fig. 5(b) and (c)). Note than the increase in w means a decrease in  $n_p$ . Therefore, the flow properties for porous media with rough solid obstacles begin to return to those for porous media with smooth solid obstacles above a threshold value of the roughness particle spacing. The trends for  $F_{pressure}$ ,  $F_{viscous}$  and Nu with respect to w are similar for all of the values of porosity tested here.

When the roughness particle spacing is increased, the flow inside the roughness cavity changes in response to the width of the cavity. At  $w = 2k_s$ , the width of the roughness cavity is equal to the roughness particle height leading to the formation of a single recirculating vortex inside the roughness cavity. The size of the recirculation zone is identical to the roughness particle height  $k_s$ . When the w is increased to  $4k_s$ , a pair of recirculating vortices are formed behind the roughness particle and in front of the neighboring roughness particle. The flow above the roughness layer is not completely bridged over the roughness layer at  $w = 4k_s$  as is the case at  $w = 2k_s$ . The flow enters the roughness cavity and increases stagnation pressure at the front face of the roughness particle leading to a higher pressure drag. The increase in the solid obstacle surface area covered by recirculating flow decreases viscous drag and Nusselt number. We have called this type of surface roughness as the densely distributed surface roughness. When w is increased further to  $8.33k_s$  and  $16.67k_s$ , the flow reattaches inside the roughness cavity following the recirculating vortex. The reattached flow then stagnates at the front face of the neighboring roughness particle that is at a downstream location. We have called this process of recirculation, reattachment, and stagnation as "tripping" hereafter. Flow tripping by sparsely distributed roughness particles increases the stagnation pressure leading to a higher pressure drag from the front face of the roughness particles (Fig. 5(d)). However, there are few roughness particles for rough solid obstacles with  $w = 8.33k_s$  and  $16.67k_s$ , which causes the pressure and viscous drag forces and the Nusselt number to approach that of the smooth solid obstacle. We have called this type of surface roughness as the sparsely distributed surface roughness.

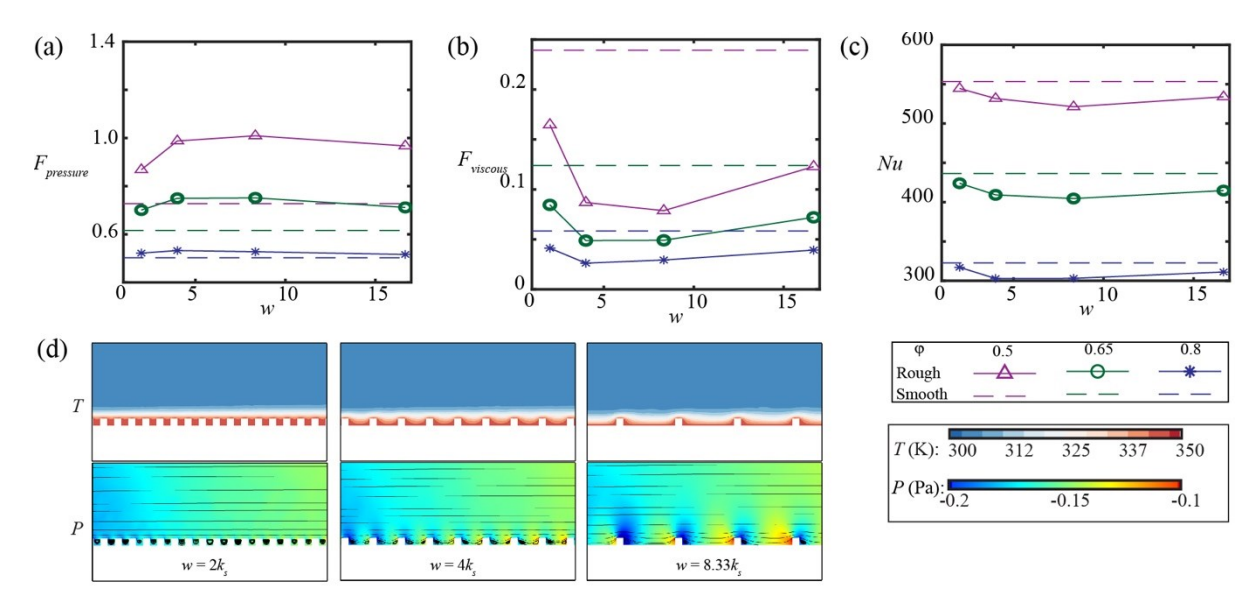


**Fig. 5** The variation of (a) pressure drag force, (b) viscous drag force, and (c) surface averaged Nusselt number is non-monotonic when the roughness particle spacing is increased. (d) The microscale temperature and pressure distributions for different values of roughness particle spacing.

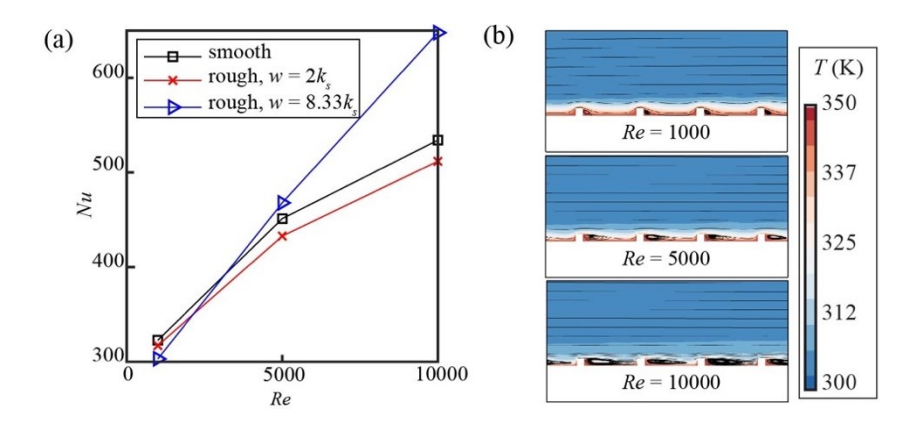


**Fig. 6** (a) The variation of the surface averaged Nusselt number with the Reynolds number for smooth and rough solid obstacles with different roughness particle spacing. (b) The microscale temperature distribution for sparsely distributed roughness ( $w = 8.33k_s$ ) shows decrease in thermal boundary layer width when the Reynolds number is increased.

The increase in the Reynolds number decreases the pressure and viscous drag forces for both the densely and sparsely distributed roughness types. There is a cross-over of the Nusselt number for the sparsely distributed roughness type when compared to the densely distributed roughness type and the smooth case (Fig. 6(a)). At Re = 1000, the Nusselt number for the sparsely distributed roughness type ( $w = 8.33k_s$ ) is less than that for the densely distributed roughness type ( $w = 2k_s$ ), which is less than that of the smooth case as described in section 3.1. At Re = 5000 and 10000, the Nusselt number for the  $w = 8.33k_s$  case is higher than that for the  $w = 2k_s$  and the smooth cases. The cross-over from heat transfer reduction to enhancement for the sparsely distributed roughness type at high Reynolds number takes place due to the following two reasons. The thermal boundary layer width inside the roughness cavity decreases in the reattached flow region when the Reynolds number increases (Fig. 6(b)). The stagnation of the reattached flow at the front face of the roughness particle causes the increase in the heat flux from the roughness particle to the flow around it. When combined, the two phenomena increase the Nusselt number for the sparsely distributed roughness type solid obstacles such that it is greater than either the densely distributed roughness type or the smooth solid obstacles.

## 4. CONCLUSIONS

In this paper, solid obstacle surface roughness has been shown to be an important consideration in the design and modeling of turbulent heat transfer in porous media. The effect of solid obstacle surface roughness on the drag force and Nusselt number is dependent on the size and distribution of the roughness particles. We have identified two regimes of solid obstacle surface roughness with respect to the roughness particle height: fine and coarse roughness regimes. In the fine roughness regime, the roughness particle height is small causing the effect of surface roughness to be limited to the boundary layer surrounding the solid obstacle surface. Roughness particles cause flow recirculation in the roughness cavity, which decreases both the velocity and temperature gradients in the wall normal direction. As a result, the viscous drag force and the Nusselt number decrease for rough solid obstacles in the fine roughness regime when compared to those of the smooth solid obstacles. The decrease in the viscous drag force causes the total drag force to be less for the rough solid obstacle with the smallest roughness particles when compared to the smooth solid obstacle. In the fine roughness regime, the roughness particles also limit the decrease in the thermal boundary layer width to the height of the roughness layer when the Reynolds number is increased. In the coarse roughness regime, the roughness particle is large enough to modify the shape of the solid obstacle and protrude deep into the pore space in between the solid obstacles. The effect of the surface roughness is prevalent in the entire pore volume since it substantially decreases the cross-sectional area through which the fluid flows. The recirculating vortex in the roughness cavity entrains cold fluid from above the roughness layer and increases the Nusselt number when compared to the smooth case. However, the increase in the Nusselt number is accompanied by an increase in the drag force.

We have segregated solid obstacle surface roughness into two types based on the roughness particle spacing: densely and sparsely distributed roughness. Densely distributed roughness has numerous roughness particles placed close to one another such that the width of the roughness cavity is less than 2 times the roughness height. In this case, the entire surface of the roughness cavity is covered with recirculating flow leading to decrease in the viscous drag and the Nusselt number. The effect of surface roughness on the heat transfer and drag forces is primarily determined by the recirculating flow in the roughness cavity. When the width of the roughness cavity is equal to the roughness particle height, the entire roughness cavity is occupied by a recirculating vortex that bridges the flow above the roughness layer enters the roughness cavity, which increases the pressure drag. For the sparsely distributed roughness, the width of the roughness cavity is large enough for the flow to reattach in the roughness cavity after recirculation behind the roughness particle. Flow reattachment is followed by stagnation at the front face of the neighboring roughness particle. This tripping of the flow by the roughness particles causes increased drag, but it is not significant since there are too few roughness particles in the sparsely distributed rough solid obstacle surface.

We have demonstrated the possibility of heat transfer enhancement in porous media using rough solid obstacles. The heat transfer enhancement comes at the cost of increased drag force on the solid obstacle surface. The increased drag force can be overcome by varying the roughness particle height and spacing, as well as the Reynolds number. Rough solid obstacles in the fine roughness regime incur low additional drag due to roughness. The limitation of the boundary layer thickness by the roughness particle height for the fine roughness regime can be overcome by using sparsely distributed roughness to cause flow reattachment and by simultaneously increasing the Reynolds number. There is a lot of scope for future work since the flow field is strongly dependent on the microscale solid obstacle geometry. The variation of the aspect ratio, the dimensionality, and the shape of the roughness particle will provide further insight.

#### **ACKNOWLEDGEMENTS**

AVK acknowledges the support of the National Science Foundation (award CBET-2042834) and the Alexander Humboldt Foundation Research Award.

#### **NOMENCLATURE**

d	hydraulic diameter of the	[m]	μ	dynamic viscosity	$[Ns/m^2]$
	smooth solid obstacle		Re	Reynolds number	[ ]
$k_s$	roughness particle height	[m]	$u_m$	Reynolds and superficially	[m/s]
w	roughness particle spacing	[m]		(over the whole volume)	
$n_p$	number of roughness particles	[ ]		averaged x- velocity	
	along one side of the obstacle		$\Delta x$	maximum grid size	[m]
S	pore size	[m]	$F_{pressure}$	pressure drag force acting on	[N]
φ	porosity	[ ]		the solid obstacle surface	
$g_x$	applied pressure gradient term	$[m/s^2]$	$F_{viscous}$	viscous drag force acting on	[N]
$T_w$	temperature at the solid	[K]		the solid obstacle surface	
	obstacle surface		Nu	Nusselt number averaged over	[ ]
$T_{in}$	bulk temperature of the fluid	[K]		the solid obstacle surface	
	entering the periodic domain		$q''_w$	heat flux averaged over the	$[W/m^2]$
λ	fluid thermal conductivity	[W/mK	.]	solid obstacle surface	
$C_P$	fluid specific heat	J/KgK	]		
ρ	fluid density	[Kg/m <sup>3</sup>	]		

#### REFERENCES

- [1] A. Mehmani, S. Kelly, C. Torres-Verdín, M. Balhoff, Capillary Trapping Following Imbibition in Porous Media: Microfluidic Quantification of the Impact of Pore-Scale Surface Roughness, Water Resour. Res. 55 (2019) 9905–9925. https://doi.org/10.1029/2019WR025170.
- [2] X. Lyu, X. Liu, Y. Sun, B. Gao, R. Ji, J. Wu, Y. Xue, Importance of surface roughness on perfluorooctanoic acid (PFOA) transport in unsaturated porous media, Environ. Pollut. 266 (2020) 115343. https://doi.org/10.1016/j.envpol.2020.115343.
- [3] L. Zhang, C. Xu, Y. Guo, G. Zhu, S. Cai, X. Wang, W. Jing, H. Sun, Y. Yang, J. Yao, The Effect of Surface Roughness on Immiscible Displacement Using Pore Scale Simulation, Transp. Porous Media. 140 (2021) 713–725. https://doi.org/10.1007/s11242-020-01526-6.
- [4] S. Yang, M. Liang, B. Yu, M. Zou, Permeability model for fractal porous media with rough surfaces, Microfluid. Nanofluidics. 18 (2015) 1085–1093. https://doi.org/10.1007/s10404-014-1500-1.
- [5] T.A. Cousins, B. Ghanbarian, H. Daigle, Three-Dimensional Lattice Boltzmann Simulations of Single-Phase Permeability in Random Fractal Porous Media with Rough Pore–Solid Interface, Transp. Porous Media. 122 (2018) 527–546. https://doi.org/10.1007/s11242-017-0938-5.
- [6] S. Pasquier, M. Quintard, Y. Davit, Modeling flow in porous media with rough surfaces: Effective slip boundary conditions and application to structured packings, Chem. Eng. Sci. 165 (2017) 131–146. https://doi.org/10.1016/j.ces.2017.01.063.
- [7] E. Achenbach, Heat transfer from smooth and rough in-line tube banks at high Reynolds number, Int. J. Heat Mass Transf. 34 (1991) 199–207. https://doi.org/10.1016/0017-9310(91)90186-I.
- [8] G.F.K. Tay, D.C.S. Kuhn, M.F. Tachie, Surface roughness effects on the turbulence statistics in a low Reynolds number channel flow, J. Turbul. 14 (2013) 121–146. https://doi.org/10.1080/14685248.2012.737468.
- [9] Y.K. Choi, H.G. Hwang, Y.M. Lee, J.H. Lee, Effects of the roughness height in turbulent boundary layers over rodand cuboid-roughened walls, Int. J. Heat Fluid Flow. 85 (2020) 108644. https://doi.org/10.1016/j.ijheatfluidflow.2020.108644.
- [10] Y. Miyake, K. Tsujimoto, Y. Agata, A DNS of a Turbulent Flow in a Rough-Wall Channel Using Roughness Elements Model, JSME Int. J. Ser. B. 43 (2000) 233–242. https://doi.org/10.1299/jsmeb.43.233.
- [11] Y. Jin, H. Herwig, Turbulent flow and heat transfer in channels with shark skin surfaces: Entropy generation and its physical significance, Int. J. Heat Mass Transf. (2014). https://doi.org/10.1016/j.ijheatmasstransfer.2013.10.063.
- Y. Nagano, H. Hattori, T. Houra, DNS of velocity and thermal fields in turbulent channel flow with transverse-rib roughness, Int. J. Heat Fluid Flow. 25 (2004) 393–403. https://doi.org/10.1016/j.ijheatfluidflow.2004.02.011.
- [13] K. Katoh, K.-S. Choi, T. Azuma, Heat-transfer enhancement and pressure loss by surface roughness in turbulent channel flows, Int. J. Heat Mass Transf. 43 (2000) 4009–4017. https://doi.org/10.1016/S0017-9310(00)00033-8.
- [14] I. Rodriguez, O. Lehmkuhl, U. Piomelli, J. Chiva, R. Borrell, A. Oliva, Numerical simulation of roughness effects on the flow past a circular cylinder, J. Phys. Conf. Ser. 745 (2016) 32043. https://doi.org/10.1088/1742-6596/745/3/032043.
- [15] L. Jiang, H. Shan, J. Mansfield, K. Junghans, E. Harrison, LES of Flow Past a Circular Cylinder With Roughened Surface, in: Proc. ASME 2017 Fluids Eng. Div. Summer Meet., Waikoloa, Hawaii, USA, 2017: p. V01BT12A006. https://doi.org/10.1115/FEDSM2017-69326.
- [16] Y. Yamagishi, M. Oki, Numerical simulation of flow around a circular cylinder with curved sectional grooves, J. Vis. 10 (2007) 179–186. https://doi.org/10.1007/BF03181829.
- [17] J. Zhao, Z. Wang, P. Guo, Q. Luo, Molecular level investigation of methane and carbon dioxide adsorption on SiO2 surface, Comput. Mater. Sci. (2019). https://doi.org/10.1016/j.commatsci.2019.05.044.
- [18] F. Dierich, P.A. Nikrityuk, A numerical study of the impact of surface roughness on heat and fluid flow past a cylindrical particle, Int. J. Therm. Sci. (2013). https://doi.org/10.1016/j.ijthermalsci.2012.08.009.
- [19] X. Chu, G. Yang, S. Pandey, B. Weigand, Direct numerical simulation of convective heat transfer in porous media, Int. J. Heat Mass Transf. 133 (2019) 11–20. https://doi.org/10.1016/j.ijheatmasstransfer.2018.11.172.
- [20] M.F. Uth, Y. Jin, A. V. Kuznetsov, H. Herwig, A direct numerical simulation study on the possibility of macroscopic turbulence in porous media: Effects of different solid matrix geometries, solid boundaries, and two porosity scales, Phys. Fluids. 28 (2016) 065101. https://doi.org/10.1063/1.4949549.
- [21] T.H. Shih, W.W. Liou, A. Shabbir, Z. Yang, J. Zhu, A new k-ε turbulent eddy viscosity model for high reynolds number turbulent flows, 1995. https://doi.org/10.1016/0045-7930(94)00032-T.
- [22] H.C. Chen, V.C. Patel, Near-wall turbulence models for complex flows including separation, AIAA J. (1988). https://doi.org/10.2514/3.9948.
- [23] ANSYS Inc., ANSYS FLUENT Theory Guide, Release 17.2. (2016).
- [24] M. Cascetta, G. Cau, P. Puddu, F. Serra, A comparison between CFD simulation and experimental investigation of a packed-bed thermal energy storage system, Appl. Therm. Eng. 98 (2016) 1263–1272. https://doi.org/10.1016/j.applthermaleng.2016.01.019.
- [25] F.A. Rodrigues, M.J.S. de Lemos, Effect of porous material properties on thermal efficiencies of a thermocline storage tank, Appl. Therm. Eng. 173 (2020) 115194. https://doi.org/10.1016/j.applthermaleng.2020.115194.
- [26] X. Chu, B. Weigand, V. Vaikuntanathan, Flow turbulence topology in regular porous media: From macroscopic to microscopic scale with direct numerical simulation, Phys. Fluids. 30 (2018) 065102. https://doi.org/10.1063/1.5030651.
- [27] V. Srikanth, C.-W. Huang, T.S. Su, A. V Kuznetsov, Symmetry breaking of turbulent flow in porous media composed of periodically arranged solid obstacles, J. Fluid Mech. 929 (2021) A2. https://doi.org/10.1017/jfm.2021.813.